Specific Monitoring of Excited-State Symmetry-Breaking by Femtosecond Broadband Fluorescence Upconversion Spectroscopy

Joseph S. Beckwith,[†] Arnulf Rosspeintner,[†] Giuseppe Licari,[†] Markus Lunzer,[‡] Brigitte Holzer,[‡] Johannes Fröhlich,[‡] and Eric Vauthey*[,†]

†*Physical Chemistry Department, University of Geneva, Quai Ernest Ansermet 30, CH-1211 Geneva, Switzerland*

‡*Institute of Applied Synthetic Chemistry, TU Wien, Getreidemarkt 9/163OC, A-1060 Vienna, Austria*

E-mail: eric.vauthey@unige.ch

S1. Experimental Details

S1.1 One-Photon Absorption and Fluorescence Spectra

Absorption spectra were recorded on a Cary 50 absorption spectrometer. Emission spectra were collected on a Horiba Fluoromax at a controlled temperature of 20 °C. Absorption and emission spectra were baseline corrected by subtracting the spectra of the corresponding pure solvent. Absorption spectra were obtained using samples with a maximal absorbance of 1, whilst the maximal absorbance for obtaining emission spectra was kept below 0.3. The emission spectra were corrected for the wavelength sensitivity of the spectrometer used by using a set of secondary fluorescence standards.[1] Emission quantum yields were obtained using Rhodamine 6G in degassed ethanol as a secondary emission standard (fluorescence quantum yield = 0.95)[2] and using equation S1

$$\Phi_{\mathrm{s}} = \Phi_{\mathrm{r}} \frac{n_{\mathrm{s}}^2}{n_{\mathrm{r}}^2} \frac{\int I_{\mathrm{s}}(\lambda)\mathrm{d}\lambda}{\int I_{\mathrm{r}}(\lambda)\mathrm{d}\lambda} \frac{A_{\mathrm{r}} \cdot 10^{-0.565 \cdot A_{\mathrm{r}}}}{A_{\mathrm{s}} \cdot 10^{-0.565 \cdot A_{\mathrm{s}}}} \tag{S1}$$

where Φ_x is the fluorescence quantum yield of the sample (s) and the reference (r), and I_x denotes the corresponding integrated intensity of the fluorescence spectrum. A_x is the absorbance at the excitation wavelength, with n_x denoting the refractive index of the sample (s) and reference (r) solution. 0.565 is the value to correct for the inner filter effect of the spectrometer.[3,4]

S1.2 Two-Photon Absorption Spectra

Two-photon cross sections were determined via two-photon excitation spectra using a setup similar to the one described by Makarov et al.,[5] that has been described previously.[6] The two-photon cross section at a given wavenumber, $\sigma_{\mathrm{s}}^{(2)}(\tilde{\nu})$ was calculated as follows[5]

$$\sigma_{\mathrm{s}}^{(2)}(\tilde{\nu}) = \sigma_{\mathrm{r}}^{(2)}(\tilde{\nu}) \frac{I_{\mathrm{s}}(\tilde{\nu}, \lambda_{\mathrm{obs}}) c_{\mathrm{r}} \Phi_{\mathrm{r}}(\lambda_{\mathrm{obs}})}{I_{\mathrm{r}}(\tilde{\nu}, \lambda_{\mathrm{obs}}) c_{\mathrm{s}} \Phi_{\mathrm{s}}(\lambda_{\mathrm{obs}})} \tag{S2}$$

Here $I_x(\tilde{\nu}, \lambda_{\mathrm{obs}})$ is the (two-photon excited) fluorescence intensity at excitation wavenum-

ber $\tilde{\nu}$ and observation wavelength λ_{obs} for either sample or reference ($x \in \{\mathrm{s}, \mathrm{r}\}$). c_x and $\Phi_{\mathrm{r}}(\lambda_{\mathrm{obs}})$ are the concentration and differential fluorescence quantum yield (at the observation wavelength) of sample and reference. Coumarin 153 in DMSO and Rhodamine 6G in methanol were used as in the work by the Rebane group.[7]

S1.3 Time Correlated Single Photon Counting

Lifetimes above 300 ps were measured on a home-built time-correlated single photon counting device using a 400 or 470 nm laser diode (PicoQuant) as an excitation source.[8] The time resolution, as judged from the full width at half-maximum of the instrument response function (IRF) recorded with a scattering LUDOX solution, was ∼200 ps. The samples, located in a 10 × 10 mm^2 quartz cell, had an absorbance of 0.1-0.2 at the excitation wavelength. The fluorescence time profiles were analyzed by iterative reconvolution of the IRF, with a single exponential function.

S1.4 Broadband Fluorescence Up-conversion

Fluorescence up-conversion with broadband detection was performed with a setup similar to that reported by Zhang et al.[9] In brief, excitation was performed with 100 fs pulses at 400 nm generated by frequency doubling part of the output of a standard 1 kHz Ti:Sapphire amplified system. The pump intensity on the sample was below 1 mJ/cm^2. The gate pulses were at 1340 nm and were produced by an optical parametric amplifier (TOPAS C, Light Conversion). Detection of the up-converted spectra was performed with a CCD camera (Andor, DV420A-BU). The full width at half maximum of the cross correlation of the gate with the solvent Raman signal was approximately 170 fs. Corrected time-resolved emission spectra were obtained by calibration with secondary emissive standards as described.[9] Time-resolved emission spectra were recorded as a linear time-step range from -1 to 2 ps, and a logarithmic one from 2 ps to 1 ns. The crystal orientation was set to Orientation B in the nomenclature of Gerecke et al.[10] All measurements were done at magic angle. Samples were

placed in a 1 mm cuvette with an absorbance at the excitation wavelength no greater than 0.4, and stirred by bubbling the sample with nitrogen.

S1.5 Quantum-Chemical Calculations

All calculations were performed in the gas phase at the DFT level of theory. The long-range corrected hybrid CAM-B3LYP[11] functional and the cc-pVDZ basis set were used throughout. C_2 symmetry was employed during the calculations for all the molecules. Geometrical optimizations were performed using the Gaussian09 software (Rev. D)[12] with default convergence criteria but ultra fine numerical integration grid, since a larger grid is more suitable when optimising more complex molecules with some soft modes, like ones involving the methyl substituents. Moreover, the D3 version of Grimmes dispersion[13] was included during all the calculations.

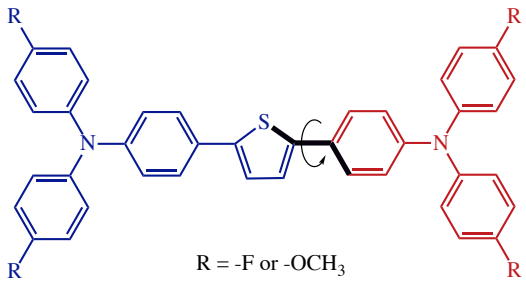

Figure S1: Structures used during the DFT simulations. The dihedral angle highlighted in bold was the angle scanned during the potential energy surface calculations.

The potential energy surface of the ground and S_1 states of **1** and **2** were obtained by rigid scan of the dihedral angle shown in Figure S1. A 0° angle corresponds to a planar conformation of the benzo-thiophene group (as shown in Figure S1). The vertical transition energies at each step were calculated from time-dependent DFT (TD-DFT).[14–16] Molecular orbitals were obtained at 0.02 isovalue.

Moreover, transition energies of the geometrically optimised single-branch analogue of **1** (**1'**) were computed as well. In the latter case, the triphenylamino group (red moiety in Figure S1) was replaced by an H atom.

S1.6 Materials and Compound Characterization

Substances purchased from commercial sources were used as received without further purification. Allyl[1,3-bis(2,6-diisopropylphenyl)imidazol-2-ylidene]chloropalladium(II) ((IPr)Pd(allyl)Cl, CAS 478980-03-9),[17] 2,5-dibromothiophene (CAS 3141-27-3)[18] and the applied boronic esters[19] were synthesized according to literature. Isopropylalcohol (IPA) was used in p.a. quality. Technical grade solvents were distilled prior to use. For the spectroscopic measurements acetonitrile (Roth, Rotidry, 99.9%), tetrahydrofuran (THF) (VWR, 99.7%, Chromanorm), n-hexane (Hexane) (Roth, Rotidry, $\geq$ 99%), dimethoxysulfoxide (DMSO) (Roth, Rotidry, $\geq$ 99.8%), Diethyl ether (Acros Organics, 99.5%, Extra Dry over Molecular Sieve), Di-n-butyl ether (Acros Organics, 99+%, Extra Dry), Ethyl Acetate (Acros Organics, 99.5%, for spectroscopy ACS), 1-Propanol (Propanol) (Alfa Aesar, Anhydrous, 99.9%), Cyclohexane (Roth, Rotisolv, HPLC, min. 99.9%), Acetone (Fischer Scientific, Analytical Reagent Grade) and methanol (MeOH) (Sigma-Aldrich, $\geq$ 99.9%, spectrophotometric grade) were used as received. Rhodamine 6G (Exciton) was used as received.

Analytical TLC was performed on Merck silica gel 60 F254 plates. Chromatographic separations at preparative scale were carried out on silica gel (Merck silica gel 60, 40 - 63 μm). Nuclear magnetic resonance (NMR) spectra were obtained using a Bruker Avance DRX-400 fourier transform spectrometer operating at the following frequencies: DRX-400: 400.1 MHz (^{1}H) and 100.6 MHz (^{13}C). The chemical shifts are reported in delta (δ) units, parts per million (ppm) downfield from tetramethylsilane using solvent residual signals for calibration. Coupling constants are reported in Hertz; multiplicity of signals is indicated by using following abbreviations: s=singlet, d=doublet, t=triplet, q=quartet. The multiplicity of ^{13}C

signals was obtained by measuring JMOD spectra. High-resolution mass spectra (HRMS) were acquired as radical cations using either a SYNAPT HDMS instrument (Waters, Manchester, UK) equipped with a matrix-assisted laser desorption/ionization (MALDI) source or a Thermo Scientific LTQ Orbitrap XL hybrid FTMS (Fourier Transform Mass Spectrometer) equipped with Thermo Fischer Exactive Plus Orbitrap (LC-ESI+) and a Shimadzu IT-TOF Mass Spectrometer. Samples for MALDI-HRMS were applied at 1 mg/mL in THF on stainless steel using nitroanthracene (3 mg/mL in THF) as MALDI matrix. All MS spectra were recorded as accurate mass data with angiotensin II (m/z = 1046.542) as internal lock mass achieving a mass accuracy of 15 - 40 ppm (i.e. Δm/z = 0.01 - 0.04 amu).

S1.7 Synthesis

General procedure for the synthesis of 1 and 2 according to Marion et al.[20] Under an argon atmosphere, 2,5-dibromothiophene 5 (1.0 eq.), boronic ester (3.0 eq.) and KOtBu (3.0 eq.) were suspended in 16 mL solvent (IPA : H2O, 3 : 1; degassed by bubbling with argon). A solution of (IPr)Pd(allyl)Cl (0.02 eq.) in degassed IPA was added and the reaction mixture was refluxed for 1.5 hours, monitoring the conversion by TLC. After completion, the reaction mixture was distributed between water and chloroform; the phases were separated and the aqueous layer was extracted with chloroform three times. The combined organic layer was dried over anhydrous sodium sulfate and the solvent removed under reduced pressure to give the crude product. Purification was achieved by column chromatography.

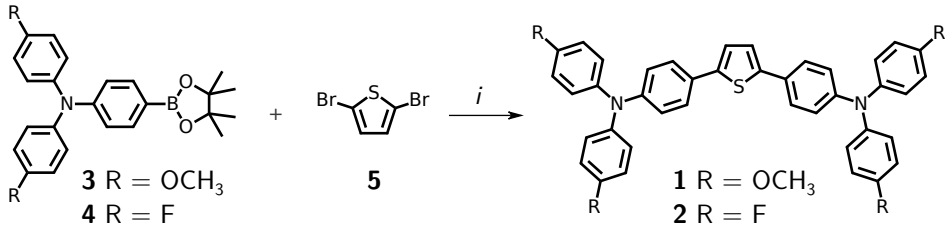

Scheme S1: Synthetic pathway to **1** and **2**. i: KOtBu, (IPr)Pd(allyl)Cl, isopropanol / water, reflux.

4,4'-(2,5-Thiophenediyl)bis[N,N-bis(4-methoxyphenyl)benzenamine] (**1**). Synthetic scheme

in scheme S1. According to the general procedure **1** was synthesized applying 2,5-dibromothiophene **5** (242 mg, 1 mmol), boronic acid pinacol ester **3** (1294 mg, 3.0 mmol), KOtBu (337 mg, 3.0 mmol) and (IPr)Pd(allyl)Cl (11.4 mg, 20 μmol; dissolved in 1 mL IPA). After general workup the crude product was purified by column chromatography (90 g silica gel, hexanes : Et_2O 30 $\rightarrow$ 100 %) and subsequently recrystallized from cyclohexane to give **1** as yellow powder (647 mg, 94 %). ^{1}H NMR (400 MHz, CD_2Cl_2): δ = 7.42 (d, J = 8.8 Hz, 4 H), 7.13 (s, 2 H), 7.10 - 7.04 (m, 8 H), 6.93 - 6.82 (m, 12 H), 3.79 (s, 12 H) ppm. ^{13}C NMR (100 MHz, CD_2Cl_2): δ = 156.7 (s), 148.7 (s), 142.9 (s), 141.1 (s), 127.3 (d), 127.0 (s), 126.5 (d), 123.1 (d), 120.9 (d), 115.2 (d), 56.0 (q) ppm. MS (MALDI-TOF): calcd for $C_{44}H_{38}N_2O_4S$: 690.2552; found: 690.2450.

4,4'-(2,5-Thiophenediyl)bis[N,N-bis(4-fluorophenyl)benzenamine] (**2**). Synthetic scheme in scheme S1. According to the general procedure **2** was synthesized applying 2,5-dibromothiophene **5** (242 mg, 1 mmol), boronic acid pinacol ester **4** (1222 mg, 3.0 mmol), KOtBu (337 mg, 3.0 mmol) and (IPr)Pd(allyl)Cl (11.4 mg, 20 μmol; dissolved in 1 mL IPA). After general workup the crude product was purified by column chromatography (90 g silica gel, cyclohexane : DCM, 15 $\rightarrow$ 20 %) and subsequently recrystallized from cyclohexane to give **2** as yellow powder (590 mg, 92 %). ^{1}H NMR (400 MHz, CD_2Cl_2): δ = 7.48 (d, J = 8.8 Hz, 4 H), 7.18 (s, 2 H), 7.14 - 6.90 (m, 20 H) ppm. ^{13}C NMR (100 MHz, CD_2Cl_2): δ = 159.6 (s, J_{CF} = 243.2 Hz), 147.9 (s), 144.1 (s, J_{CF} = 2.8 Hz), 143.0 (s), 128.6 (s), 126.9 (d, J_{CF} = 7.9 Hz), 126.8 (d), 123.7 (d), 123.0 (d), 116.7 (d, J_{CF} = 22.6 Hz) ppm. F_P = 201.5 203.5 °C. MS (MALDI-TOF): calcd for $C_{40}H_{26}F_4N_2S$: 642.1753; found: 642.1710.

Further details of the synthesis, characterisation and two-photon absorption structuring tests of the molecules **1** and **2** will be reported in an upcoming paper.[21]

S2. Steady-State Spectroscopic Data and Transition Dipole Moments

S2.1 Solvatochromism

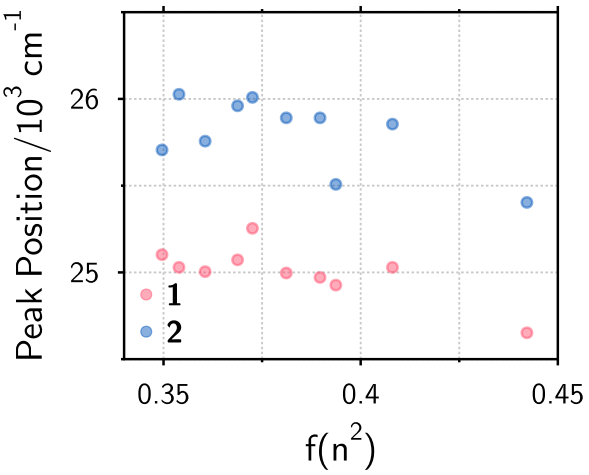

Figure S2: Absorption band maxima of **1** and **2** plotted vs $f(n^2) = 2(n^2-1)/(2n^2+1)$, where n is the refractive index.

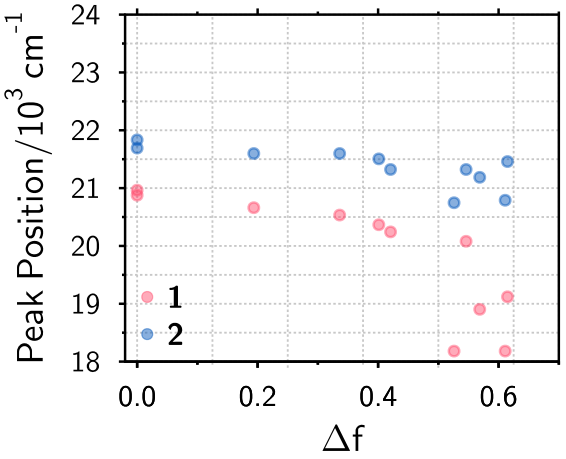

Figure S3: Fluorescence maxima of **1** and **2** plotted vs $\Delta f = 2(\epsilon-1)/(2\epsilon+1) - 2(n^2-1)/(2n^2+1)$, where n is the refractive index and ϵ is the static dielectric constant.

S2.2 Calculation of the Transition Dipole Moments

The absorption transition dipole moment was calculated using[22]

$$\mu_{abs} = 9.584 \times 10^{-2} \left[\frac{1}{n} \frac{1}{f(n)} \times \int_{S_1 band} \frac{\varepsilon(\nu)}{\nu} d\nu \right]^{1/2} \tag{S3}$$

where $\varepsilon(\nu)$ is the molar absorption coefficient of the $S_1 \leftarrow S_0$ transition and n is the refractive index of the solvent. In accordance with Toptygin,[23] $f(n)$, an effective cavity factor, is taken to be

$$f(n) = \frac{9n^2}{(2n^2+1)^2}. \tag{S4}$$

The emission dipole moment, μ_{em} was calculated using

$$\mu_{em} = 1.7857 \times 10^3 \left[\frac{1}{n^3} \frac{1}{f(n)} \frac{k_{rad}}{\tilde{\nu}_f^3} \right]^{1/2} \tag{S5}$$

where k_{rad} is the radiative rate constant in s^{-1}. Here, the radiative rate constant was calculated as $k_{rad} = \Phi_f / \tau_F$, where Φ_f is the fluorescence quantum yield and the fluorescence lifetime τ_F was determined from the analysis of the TCSPC data. As it was possible to analyse the TCSPC data using iterative reconvolution of the IRF with a single exponential function, it is assumed that any symmetry breaking at short times is not observed in the TCSPC experiments. Consequently, the fluorescence lifetime is that of the relaxed S_1 state and the resulting emission transition dipole moment corresponds to that of the symmetry-broken excited state. $\tilde{\nu}_f^3$ is the cube of the emission frequency, defined by

$$\tilde{\nu}_f^3 = \frac{\int F(\nu) \nu^{-3} d\nu}{\int F(\nu) d\nu}. \tag{S6}$$

To extract these, the absorption and fluorescence spectra were fitted with lineshape functions defined by

$$A_{abs}(\nu) \propto \nu \sum_{m=0}^{\infty} \frac{S_{abs}^m e^{-S_{abs}}}{m!} exp\left\{ \frac{-(h\nu_{abs}^0 + m\hbar\omega - h\nu)^2}{2\sigma_{abs}^2} \right\}, \tag{S7}$$

and

$$F_{em}(\nu) \propto \nu^3 \sum_{m=0}^{\infty} \frac{S_{em}^m e^{-S_{em}}}{m!} exp\left\{ \frac{-(h\nu_{em}^0 - m\hbar\omega - h\nu)^2}{2\sigma_{em}^2} \right\}, \quad \text{(S8)}$$

which represent the spectra as progressions of vibronic lines of width $\Gamma = \sigma \cdot \sqrt{8 \cdot ln2}$ built on a "0-0" frequency, ν^0, and resulting from a single harmonic mode of frequency, ω, displaced by an amount $\Delta = (2S)^{1/2}$.[24] Examples of fits for both compounds are shown in Figures S4 and S5.

Fluorescence quantum yields, fluorescence lifetimes, transition dipole moments and parameters extracted from the fits using equations S7 and S8 are listed in tables S1 and S2.

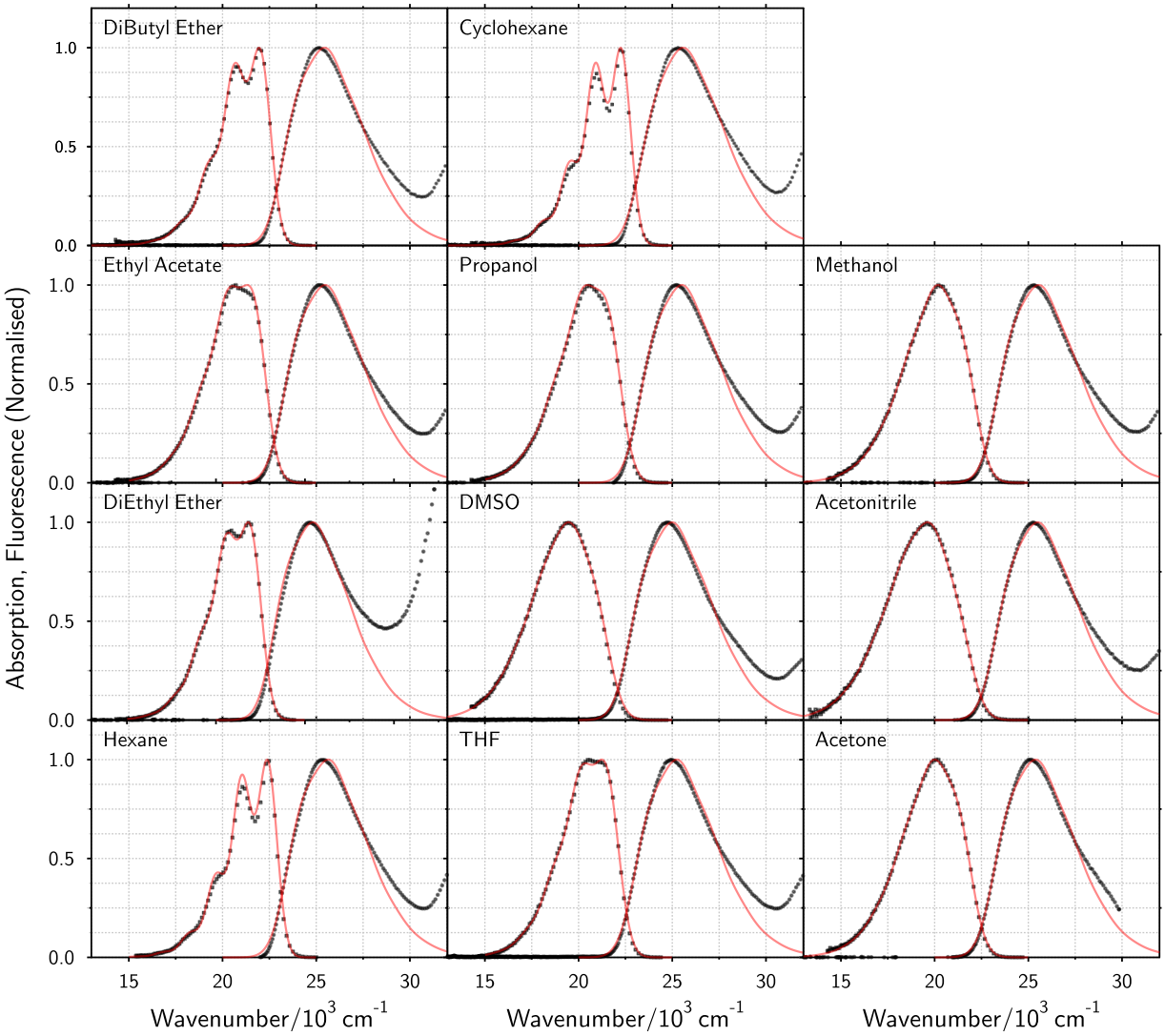

Figure S4: Steady-state absorption and emission spectra of **1** in hexane, diethyl ether, ethyl acetate, THF, DMSO, propanol, acetone, acetonitrile, methanol, cyclohexane and dibutyl ether. All spectra are shown normalized to constant peak height. The points denote the experimental spectra (thinned for ease of comparison), and the solid red curves are the fits to equations S7 and S8.

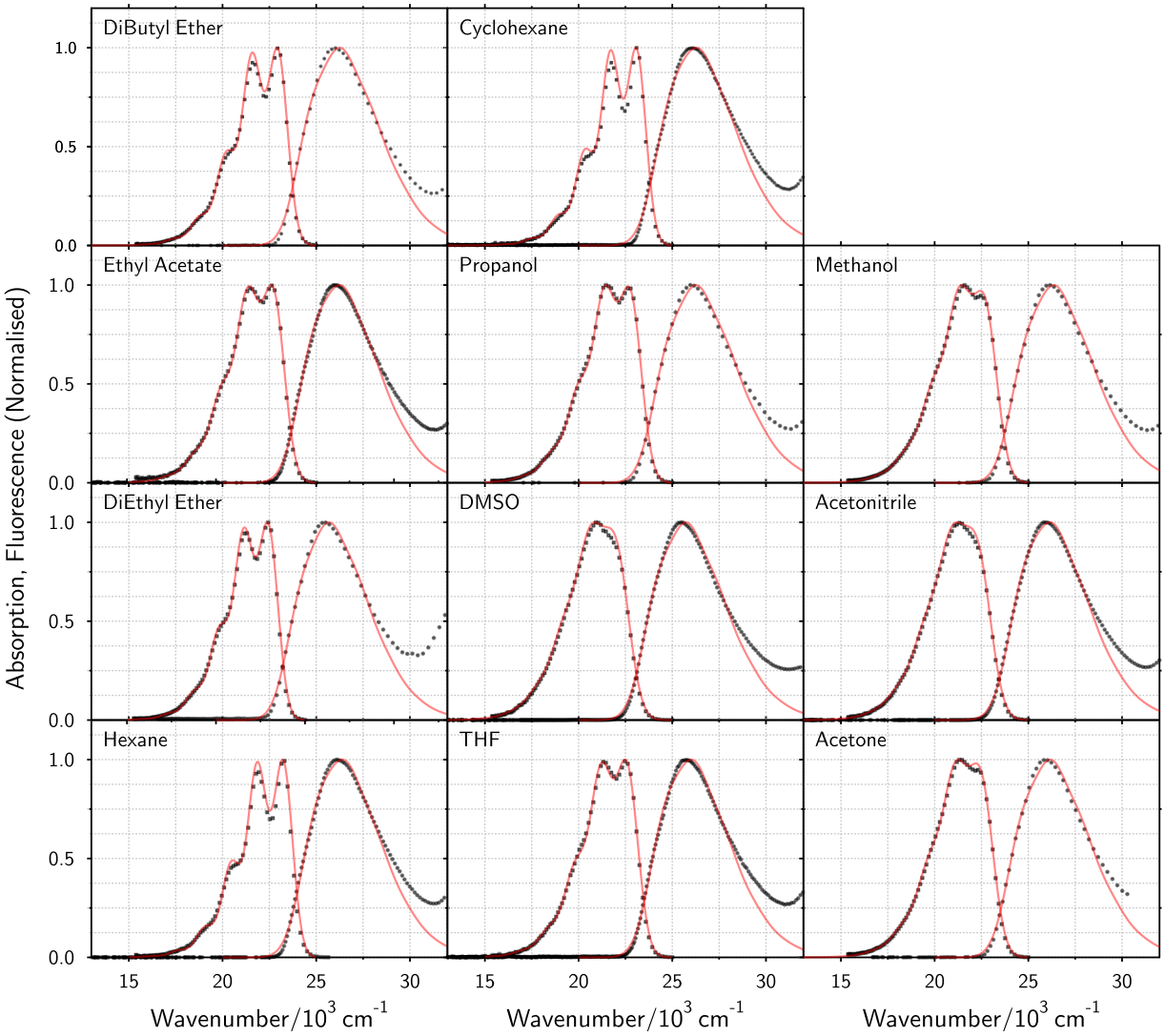

Figure S5: Steady-state absorption and emission spectra of **2** in hexane, diethyl ether, ethyl acetate, THF, DMSO, propanol, acetone, acetonitrile, methanol, cyclohexane and dibutyl ether. All spectra are shown normalized to constant peak height. The points denote the experimental spectra (thinned for ease of comparison), and the solid red curves are the fits to equations S7 and S8.

Table S1: Absorption and Fluorescence Parameters.

Compound	Solvent	Δf^a	$\varepsilon/10^{3,b}$	ν_{abs}^{max}	ν_{em}^{max}	$\Delta\nu_f$	μ_{abs}^c/D	μ_{em}^d/D	Φ_f	τ/ns
1	Hexane	0	60	25.3	21.0	0	9.85	10.23	0.31	0.54
	Cyclohexane	0	60	25.0	20.9	0.1	10.05	10.23	0.33	0.53
	DiButyl Ether	0.19	60	25.0	20.7	0.3	9.95	10.04	0.37	0.68
	DiEthyl Ether	0.34	60	25.0	20.5	0.4	10.00	9.82	0.37	0.76
	Ethyl Acetate	0.40	60	25.1	20.4	0.6	9.93	9.45	0.47	1.08
	THF	0.42	61	24.9	20.2	0.7	10.06	9.79	0.60	1.25
	DMSO	0.53	60	24.7	18.2	2.8	10.16	8.18	0.73	2.47
	Propanol	0.55	60	25.0	20.1	0.9	9.95	8.85	0.47	1.23
	Acetone	0.57	60	25.0	18.9	2.1	9.96	8.98	0.66	1.93
	Acetonitrile	0.61	60	25.1	18.2	2.8	9.96	8.61	0.71	2.59
	Methanol	0.61	60	25.1	19.1	1.8	9.91	9.04	0.56	1.65
2	Hexane	0	63	26.0	21.8	0	9.89	9.61	0.33	0.57
	Cyclohexane	0	62	25.9	21.7	0.1	10.06	9.61	0.33	0.53
	DiButyl Ether	0.19	62	25.9	21.6	0.2	10.03	9.71	0.30	0.52
	DiEthyl Ether	0.34	62	26.0	21.6	0.2	10.08	9.82	0.31	0.55
	Ethyl Acetate	0.40	62	26.0	21.5	0.3	9.98	9.75	0.32	0.59
	THF	0.42	62	25.5	21.3	0.5	10.01	10.19	0.39	0.64
	DMSO	0.53	62	25.4	20.7	1.1	10.16	9.45	0.60	1.15
	Propanol	0.55	62	25.9	21.3	0.5	10.04	9.56	0.32	0.60
	Acetone	0.57	62	25.8	21.2	0.6	10.02	9.95	0.41	0.78
	Acetonitrile	0.61	62	20.8	22.2	1.0	9.98	9.22	0.38	0.87
	Methanol	0.61	62	26.0	21.5	0.4	9.98	9.84	0.35	0.68

[a] calculated using $2(\epsilon-1)/(2\epsilon+1) - 2(n^2-1)/(2n^2+1)$ where n is the refractive index at 20°C and ϵ is the static dielectric constant at 20°C.[25] [b] in units of $M^{-1} \cdot cm^{-1}$. [c] ± 5%. [d] ± 10%. All frequencies in units of 10^3 cm^{-1}.

Table S2: Best-fit parameters of equations S7 and S8 to absorption and fluorescence spectra.

Compound	Solvent	Δf^a	ν^0_{abs}	Γ_{abs}	S_{abs}	ω_{abs}	ν^0_{em}	Γ_{em}	S_{em}	ω_{em}
1	Hexane	0	24.2	1.98	1.18	1.58	22.4	1.18	1.10	1.38
	Cyclohexane	0	24.0	2.05	1.25	1.58	22.2	1.18	1.11	1.38
	DiButyl Ether	0.19	23.9	2.00	1.20	1.58	22.0	1.30	1.09	1.38
	DiEthyl Ether	0.34	24.0	2.02	1.26	1.58	21.9	1.41	1.11	1.38
	Ethyl Acetate	0.40	24.0	2.01	1.20	1.58	21.6	1.56	1.17	1.38
	THF	0.42	23.7	1.99	1.22	1.58	21.4	1.53	1.15	1.38
	DMSO	0.53	23.5	2.00	1.24	1.58	20.8	1.85	1.79	1.38
	Propanol	0.55	24.0	2.01	1.21	1.58	21.5	1.65	1.26	1.38
	Acetone	0.57	23.9	2.02	1.20	1.58	21.2	1.75	1.54	1.38
	Acetonitrile	0.61	24.0	2.04	1.22	1.58	21.1	1.85	2.02	1.38
	Methanol	0.61	24.0	2.02	1.20	1.58	21.4	1.75	1.59	1.38
2	Hexane	0	25.0	2.05	1.16	1.56	23.2	1.18	1.18	1.39
	Cyclohexane	0	24.8	2.07	1.20	1.56	23.0	1.18	1.18	1.39
	DiButyl Ether	0.19	24.7	2.00	1.27	1.56	22.9	1.22	1.16	1.39
	DiEthyl Ether	0.34	24.8	2.02	1.32	1.56	22.9	1.27	1.15	1.39
	Ethyl Acetate	0.40	24.8	2.02	1.19	1.56	22.7	1.38	1.17	1.39
	THF	0.42	24.6	2.00	1.18	1.56	22.5	1.37	1.17	1.39
	DMSO	0.53	24.3	1.97	1.20	1.56	22.0	1.60	1.24	1.39
	Propanol	0.55	24.7	1.99	1.28	1.56	22.7	1.38	1.19	1.39
	Acetone	0.57	24.6	1.98	1.27	1.56	22.4	1.52	1.21	1.39
	Acetonitrile	0.61	24.7	2.04	1.18	1.56	22.2	1.64	1.24	1.39
	Methanol	0.61	24.8	2.01	1.26	1.56	22.6	1.49	1.23	1.39

[a] calculated using $2(\epsilon-1)/(2\epsilon+1) - 2(n^2-1)/(2n^2+1)$ where n is the refractive index at 20°C and ϵ is the static dielectric constant at 20°C.[25] All frequencies and width parameters in units of 10^3 cm^{-1}.

S2.3. Two-Photon Absorption Spectra

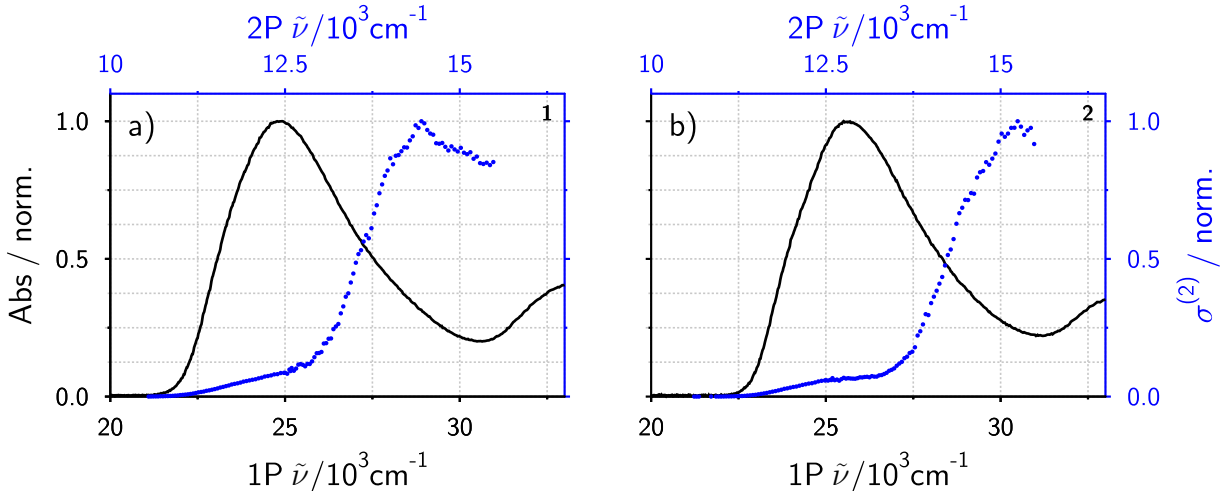

Figure S6: One-photon (black) and two-photon (blue) absorption spectra of a) **1** and b) **2**. Spectra measured in THF. $\sigma_2(14'490\text{cm}^{-1}) = 380$ GM for **1**; $\sigma_2(14'710\text{cm}^{-1}) = 300$ GM for **2**.

Table S3: Maxima of the $S_1 \leftarrow S_0$ and $S_2 \leftarrow S_0$ absorption bands.

Molecule	Solvent	$S_1 \leftarrow S_0$ / $10^3 cm^{-1}$	$S_2 \leftarrow S_0$ / $10^3 cm^{-1}$
1	Hexane	25.2	28.9
	Acetonitrile	25.2	28.9
2	Hexane	25.9	29.8
	Acetonitrile	25.8	29.8

S3. FLUPS Data and Analysis

S3.1 FLUPS Data

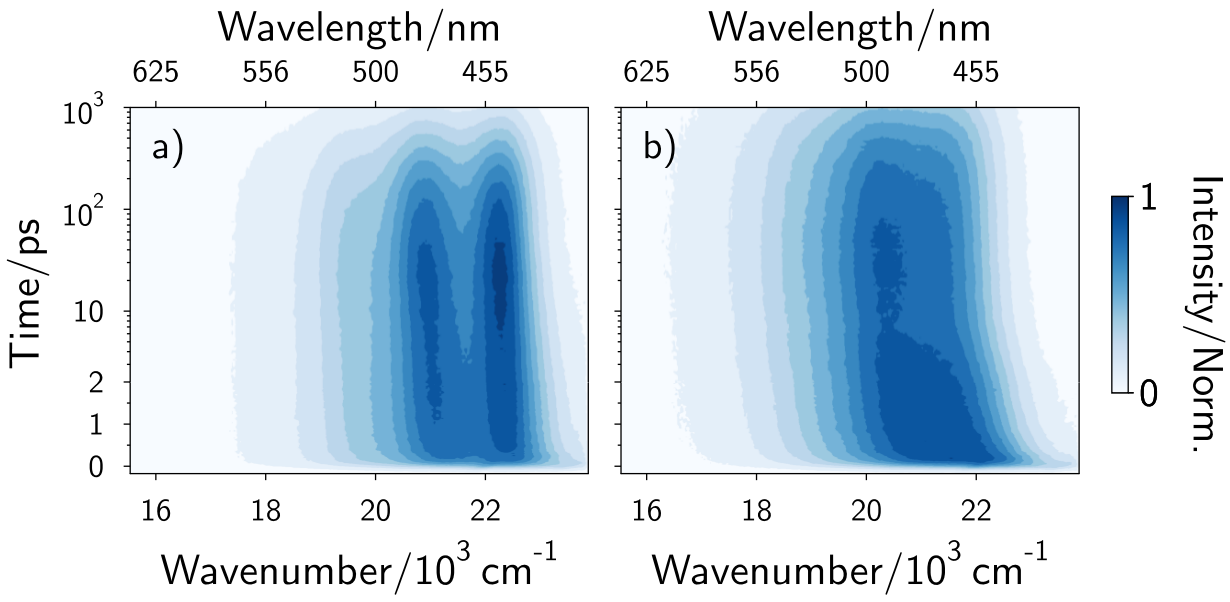

Figure S7: Time-resolved fluorescence measured with **1** in a) cyclohexane and b) THF.

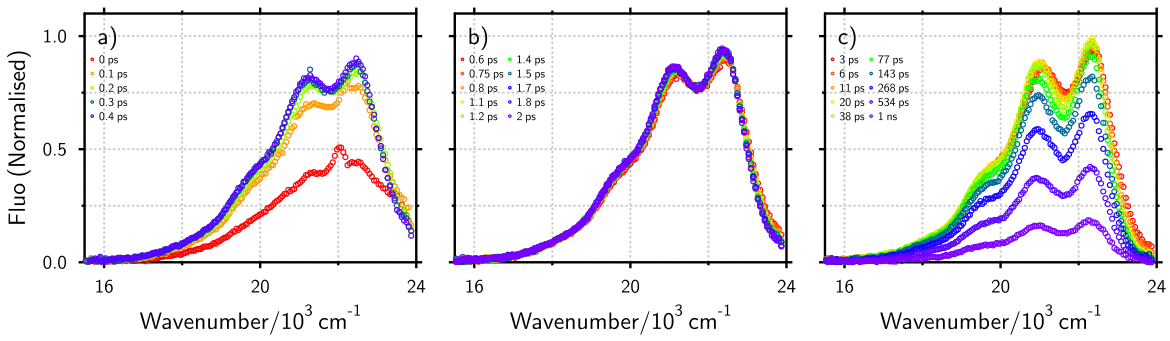

Figure S8: Transient fluorescence spectra measured with **1** in cyclohexane at different time delays. The spike a early time around 22'000 cm^{-1} is due to the Raman scattering of the solvent. These early spectra were not taken into account in the analysis.

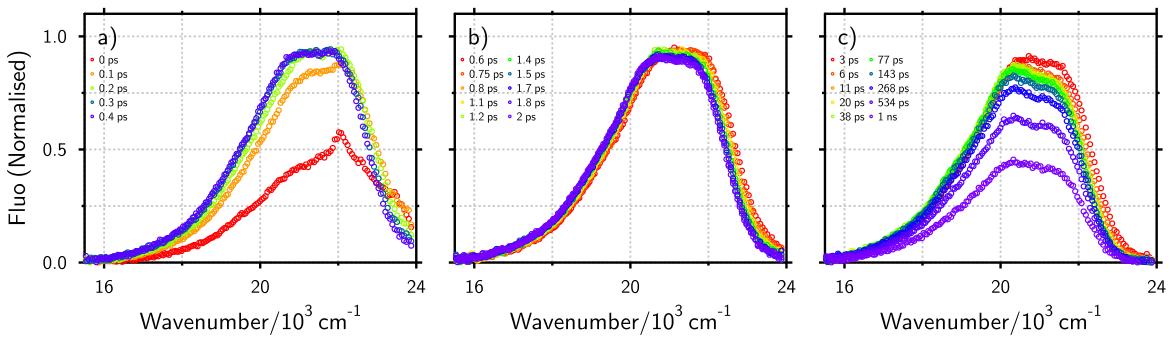

Figure S9: Transient fluorescence spectra measured with **1** in THF at different time delays.The spike a early time around 22'000 cm^{-1} is due to the Raman scattering of the solvent. These early spectra were not taken into account in the analysis.

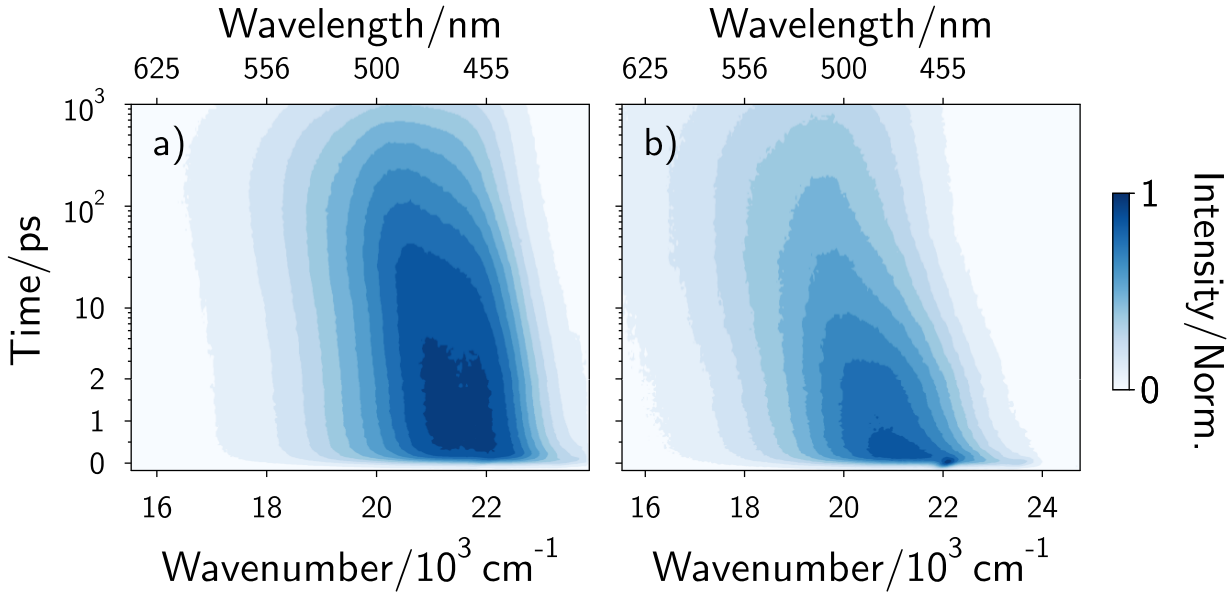

Figure S10: Time-resolved fluorescence measured with **1** in a) PrOH and b) DMSO.

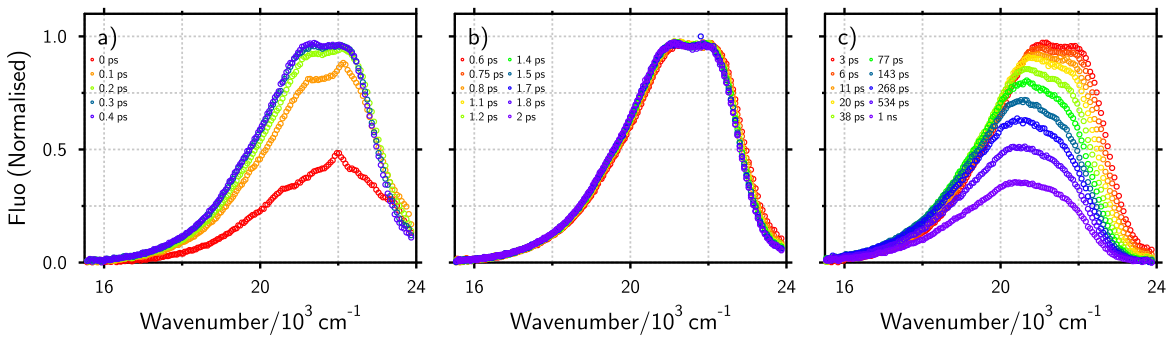

Figure S11: Transient fluorescence spectra measured with **1** in PrOH at different time delays.The spike a early time around 22'000 cm^{-1} is due to the Raman scattering of the solvent. These early spectra were not taken into account in the analysis.

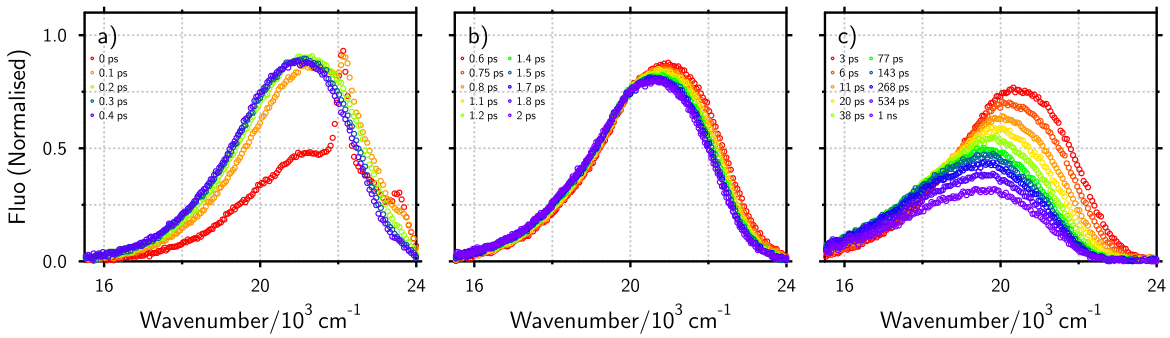

Figure S12: Transient fluorescence spectra measured with **1** in DMSO at different time delays.The spike a early time around 22'000 cm^{-1} is due to the Raman scattering of the solvent. These early spectra were not taken into account in the analysis.

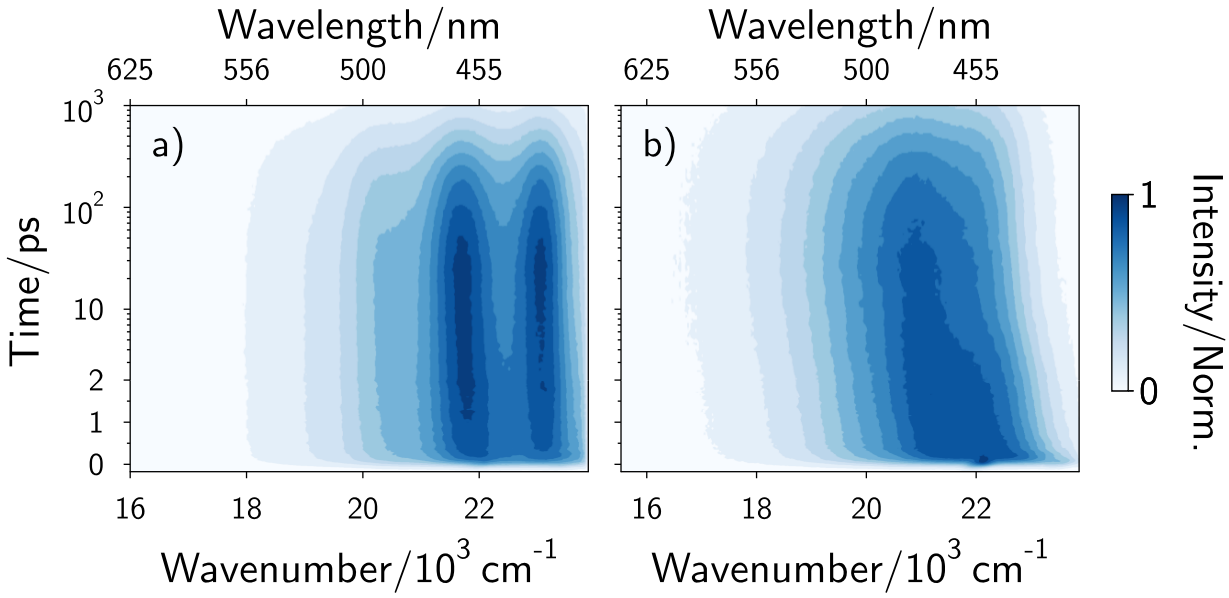

Figure S13: Time-resolved fluorescence measured with **2** in a) cyclohexane and b) DMSO.

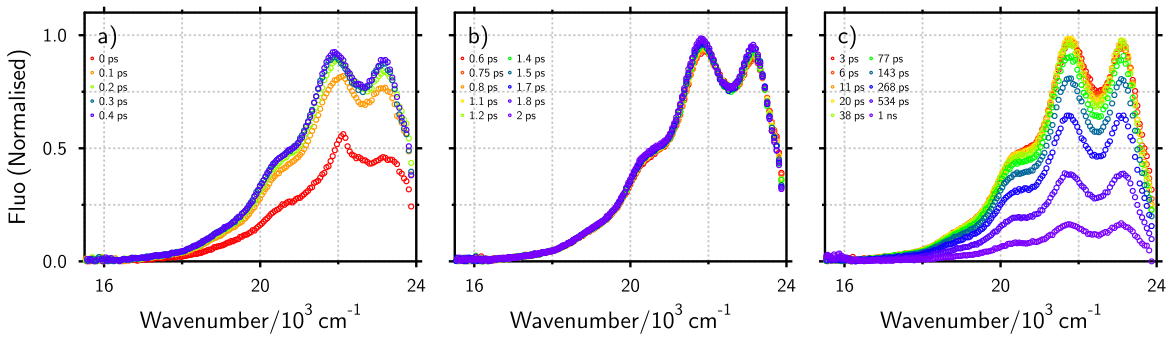

Figure S14: Transient fluorescence spectra measured with **2** in cyclohexane at different time delays.The spike a early time around 22'000 cm^{-1} is due to the Raman scattering of the solvent. These early spectra were not taken into account in the analysis.

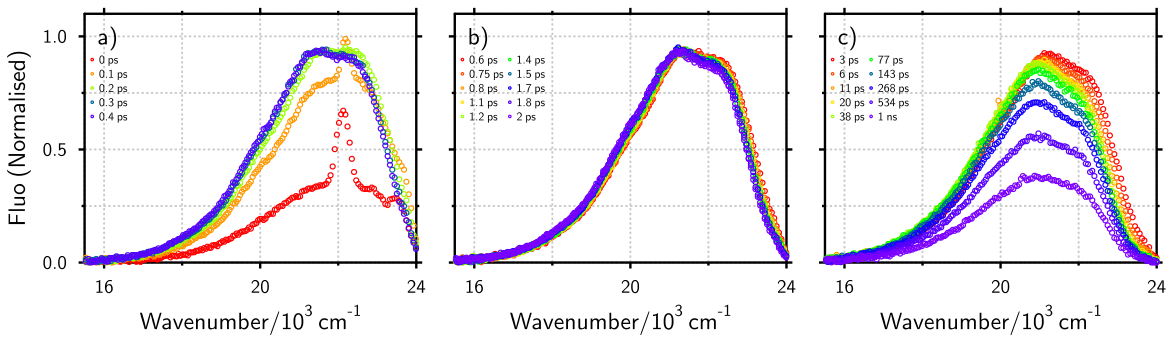

Figure S15: Transient fluorescence spectra measured with **2** in DMSO at different time delays.The spike a early time around 22'000 cm^{-1} is due to the Raman scattering of the solvent. These early spectra were not taken into account in the analysis.

S3.2 Analysis of the FLUPS spectra

The transient fluorescence spectra at each time delays were fitted with the lineshape function described in equation S8. Example of fits for each compound in each solvent are shown in Figures S16, S17, S18, S19, S20 and S21. In each case, the fit at earliest times is imperfect due to the low signal level and minor contributions of the solvent Raman peak. These early data were not taken into account. Afterward, the quality of the fit is very good. The best-fit parameters obtained from this procedure were then used to simulate the spectra over a wavenumber range from 10 to 30 $\times$ 10^3 cm^{-1} at each time delay, to ensure no fluorescence band was cut off in the subsequent analysis. The resulting spectra were then used to determine the time-resolved spectral area, which is shown together with the peak position in Figures S22, S23, S24, S25, S26 and S27. The instantaneous transition dipole moment moment was then determined by first dividing the time-resolved spectra by $e^{-(t/\tau_F)}$ to correct for the population decay (where τ_F is the fluorescence lifetime from table S1) and by $\tilde{\nu}^3$ where $\tilde{\nu}$ is the wavenumber,[26] and then by calculating the square-rooted area of the resulting spectra. The resulting area was normalised to the steady-state transition dipole moment value at long times.

This corresponds to the following equations:

$$F_\tau(t) = F(t)/e^{-(t/\tau_F)} \tag{S9}$$

where $F(t) = F(\tilde{\nu})/(\tilde{\nu}^3)$ at a particular time step, i.e. the fluorescence spectra at a time t in the transition dipole moment representation.[26] $F_\tau(t)$ is the fluorescence at a time step t corrected for population decay. In order to convert this to instantaneous transition dipole moment, this corresponds to:

$$\mu_{em}(t) = \mu_{em}(SS) \cdot \sqrt{\int_{\nu_1}^{\nu_2} F_\tau(t) / \int_{\nu_1}^{\nu_2} F_\tau(t=\infty)} \tag{S10}$$

where ν_1 and ν_2 are the start and end of the fluorescence band respectively, and $\mu_{em}(SS)$ is the transition dipole moment of emission calculated using equation S5 and the steady-state fluorescence spectra and the corresponding τ_F from table S1. $F_\tau(t=\infty)$ corresponds to the fluorescence spectrum after all relaxation occurs (at long times), i.e. it is a normalisation factor.

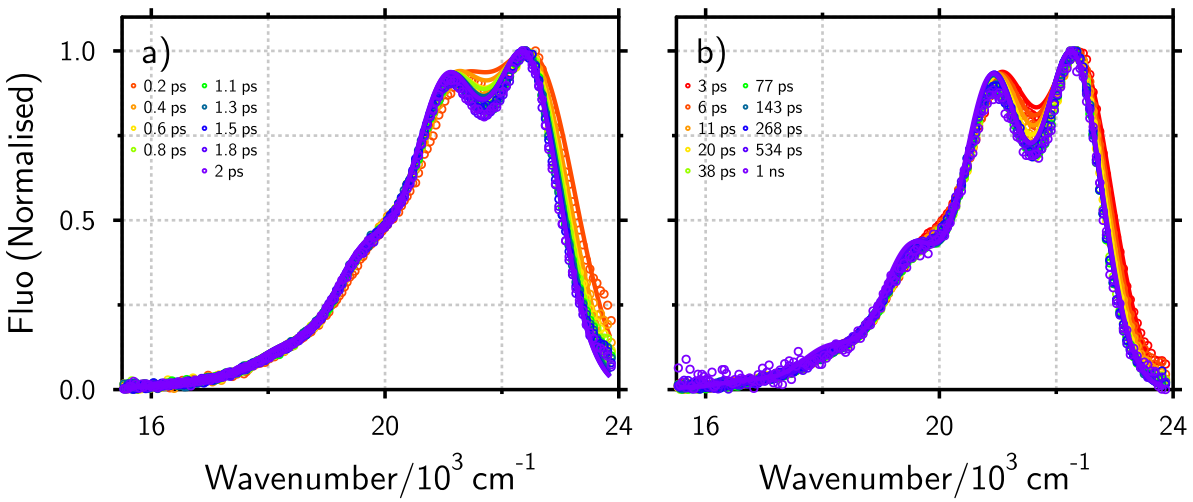

Figure S16: Comparison between the transient fluorescence spectra and the best fits of equation S8 for **1** in cyclohexane. The spectra were intensity normalized for better viewing.

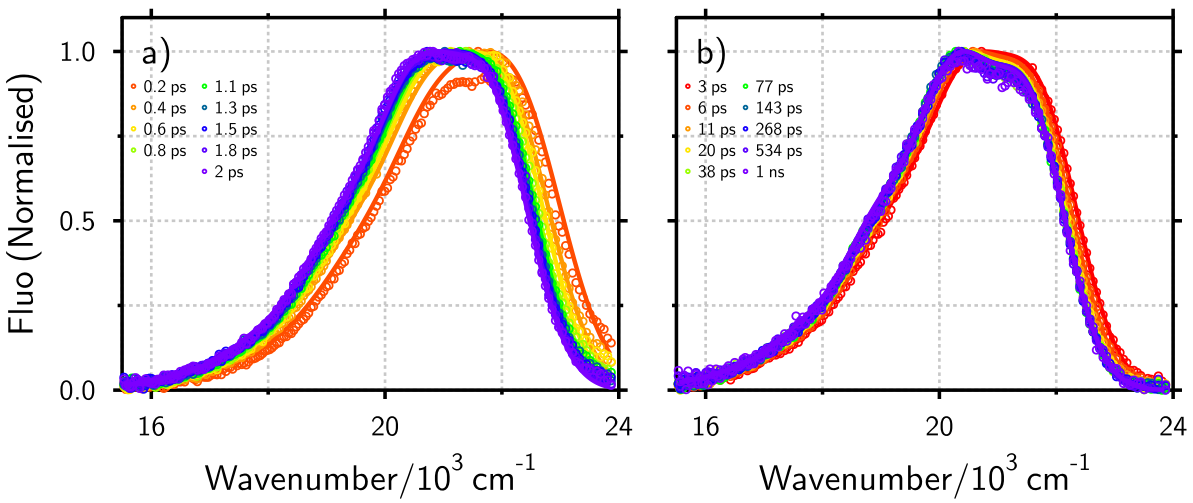

Figure S17: Comparison between the transient fluorescence spectra and the best fits of equation S8 for **1** in THF. The spectra were intensity normalized for better viewing.

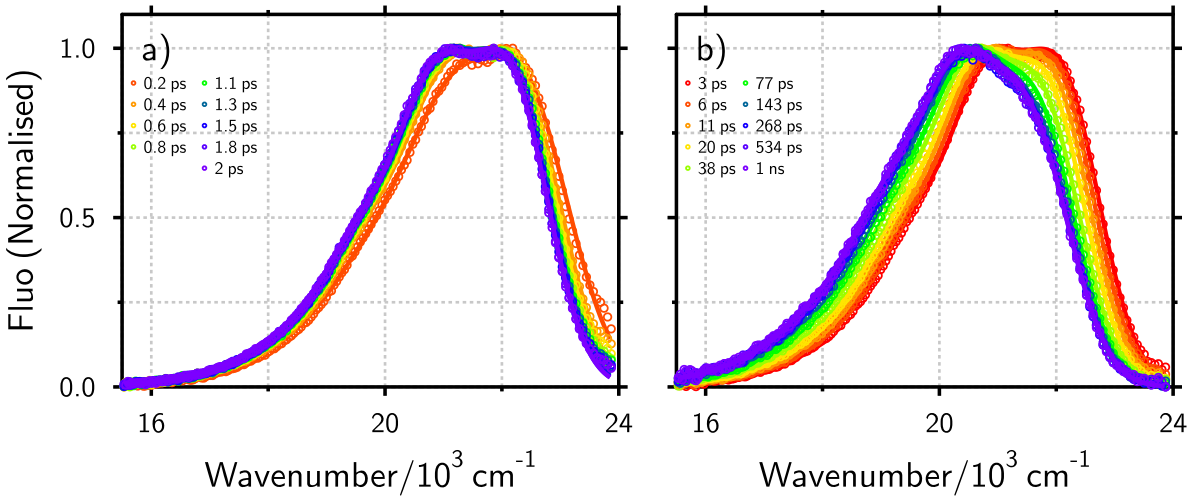

Figure S18: Comparison between the transient fluorescence spectra and the best fits of equation S8 for **1** in PrOH. The spectra were intensity normalized for better viewing

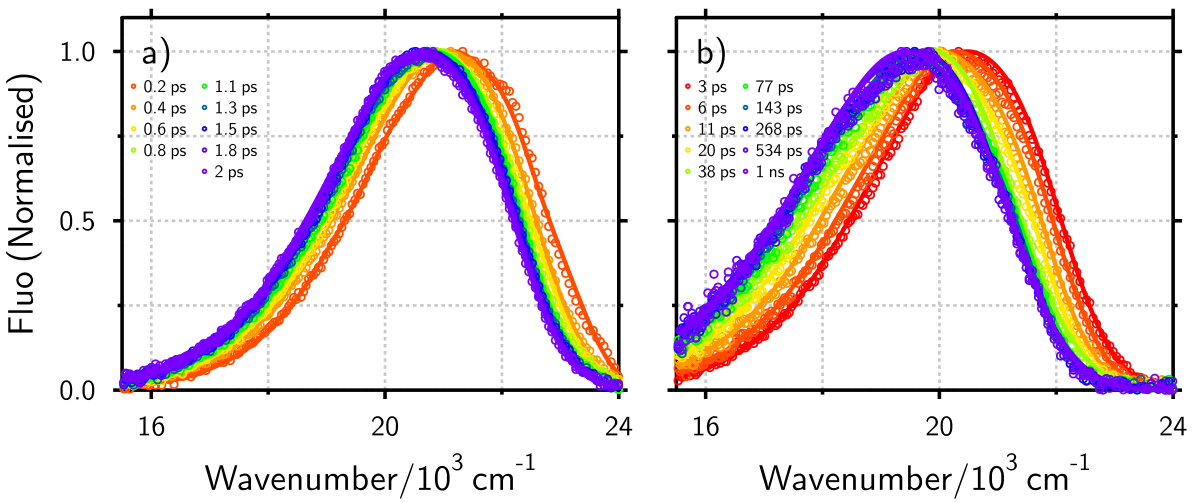

Figure S19: FLUPS data for compared to fitting with equation S8 for **1** in DMSO at a) short times and b) intermediate to long times. Peak height normalised to constant height to ease viewing of data.

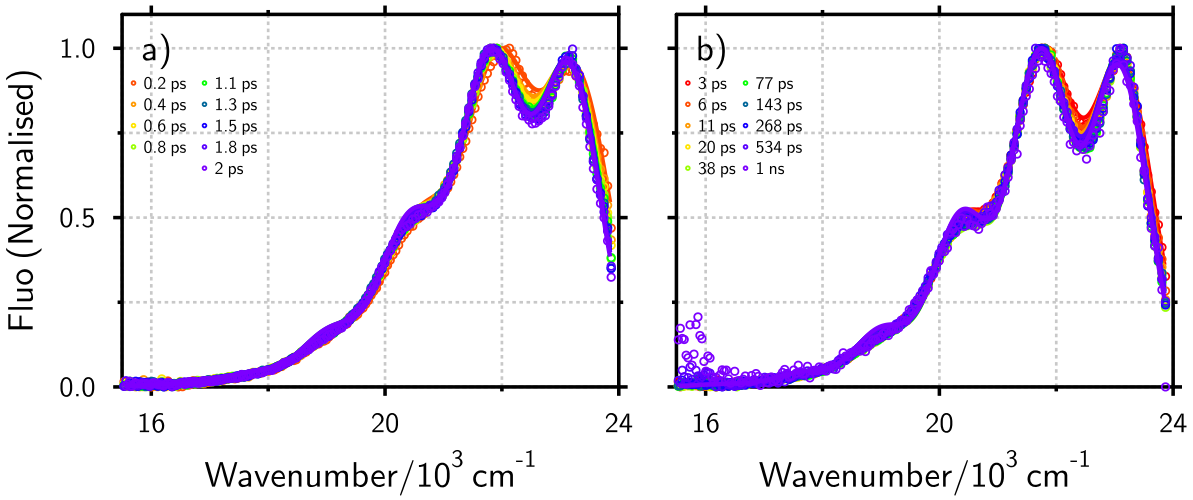

Figure S20: Comparison between the transient fluorescence spectra and the best fits of equation S8 for **2** in cyclohexane. The spectra were intensity normalized for better viewing.

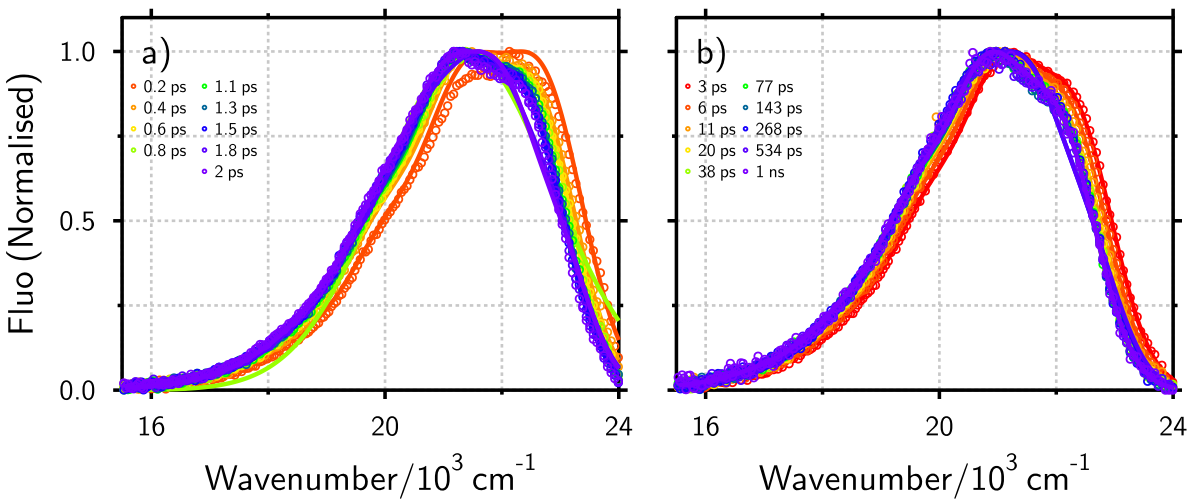

Figure S21: Comparison between the transient fluorescence spectra and the best fits of equation S8 for **2** in DMSO. The spectra were intensity normalized for better viewing.

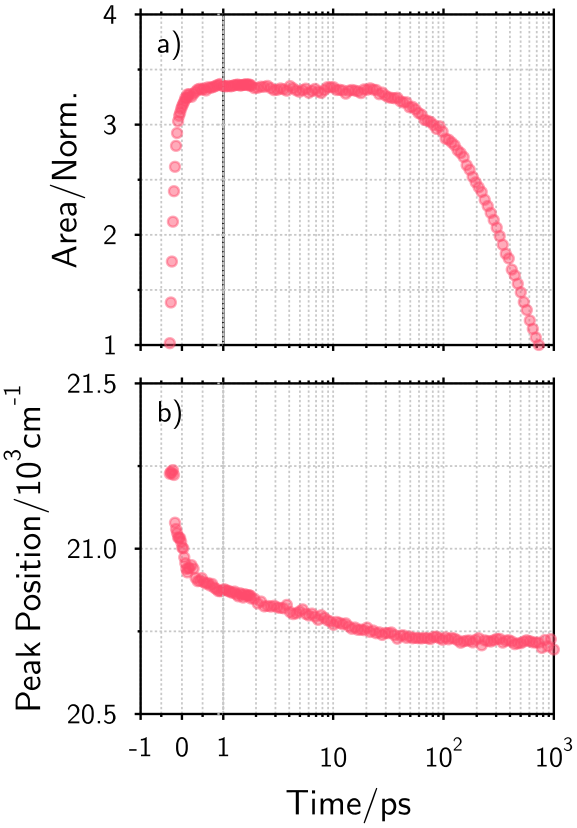

Figure S22: a) 0th and b) 1st moment of the transient emission spectra of **1** in cyclohexane.

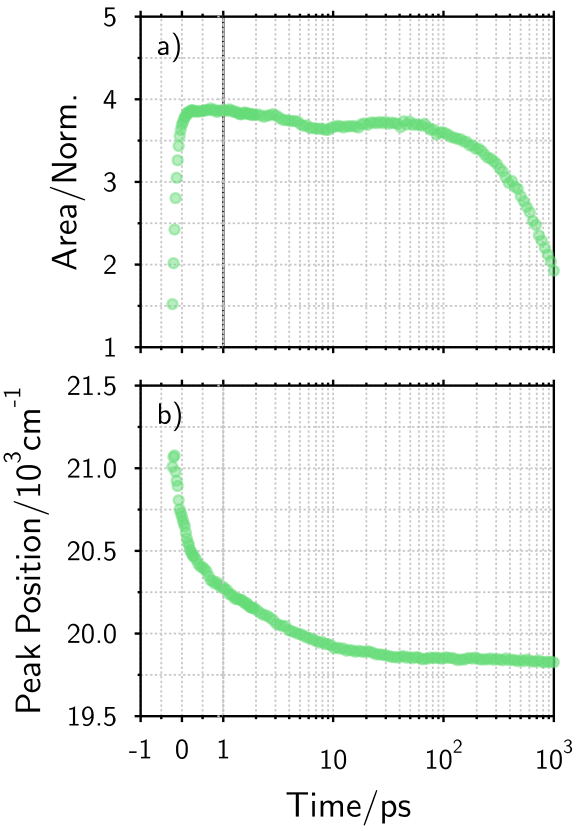

Figure S23: a) 0th and b) 1st moment of the transient emission spectra of **1** in THF.

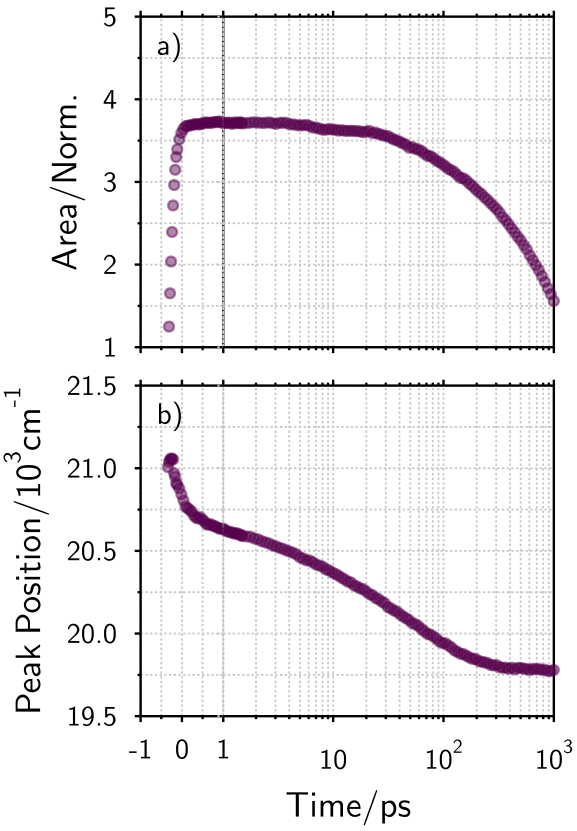

Figure S24: a) 0th and b) 1st moment of the transient emission spectra of **1** in PrOH.

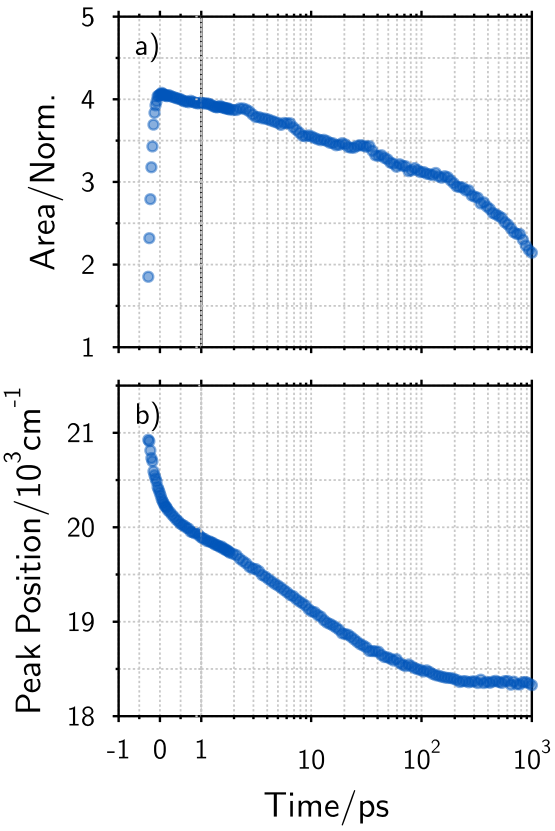

Figure S25: a) 0th and b) 1st moment of the transient emission spectra of **1** in DMSO.

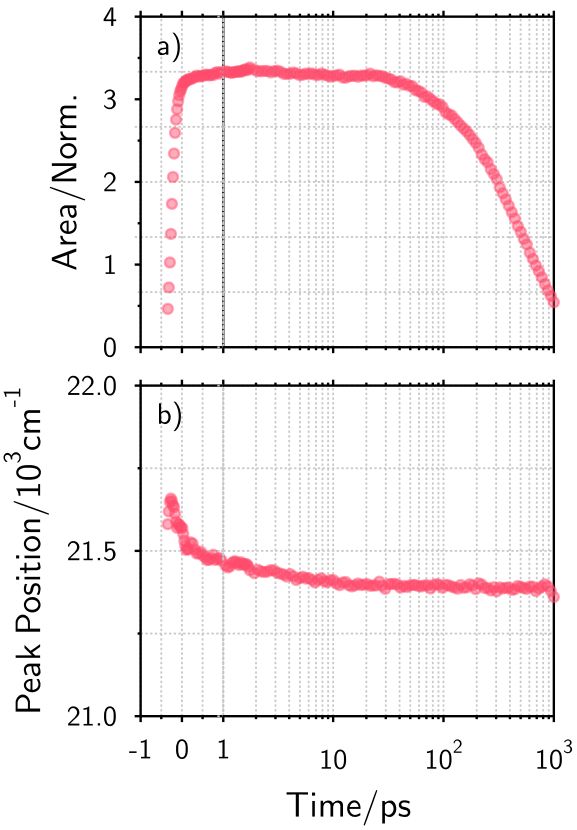

Figure S26: a) 0th and b) 1st moment of the transient emission spectra of **2** in cyclohexane.

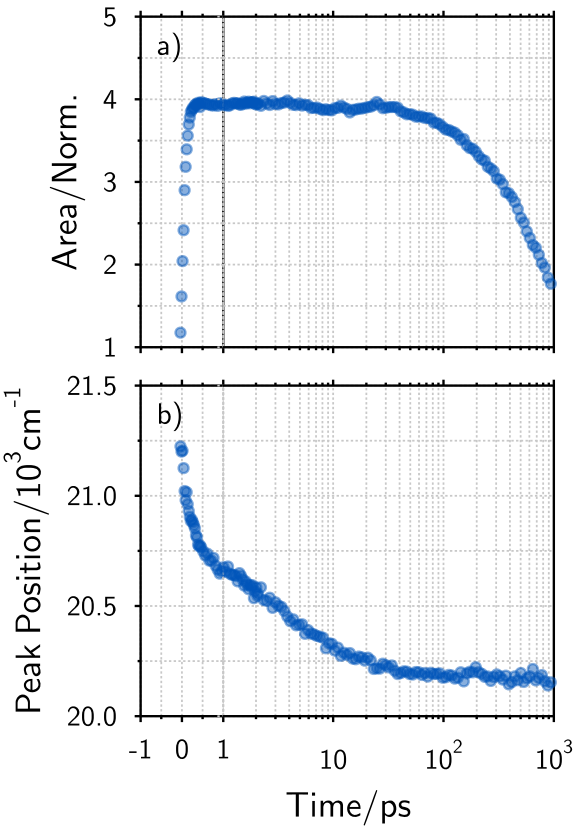

Figure S27: a) 0th and b) 1st moment of the transient emission spectra of **2** in DMSO.

S4. Quantum Chemical Calculations

S4.1 Effect of Torsion

The effect of torsion around the single bond between the central thiophene unit and an adjacent phenyl subunit (see Figure S1) on the energy of the ground state and the excited state is illusttated in Figures S28 and S29. These calculations show that the ground state minimum does not correspond to a strictly planar geometry. Moreover, they points to a relatively broad distribution of torsion angles at room temperature. However, planarization is strongly favored in the excited state, due to conjugation. This is confirmed by the DFT computed HOMO and LUMO that point to an increase of electronic density in these dihedral bonds. These figures also reveal that the $S_1 \leftarrow S_0$ transition dipole moment depends on the dihedral angle and increases with planarization.

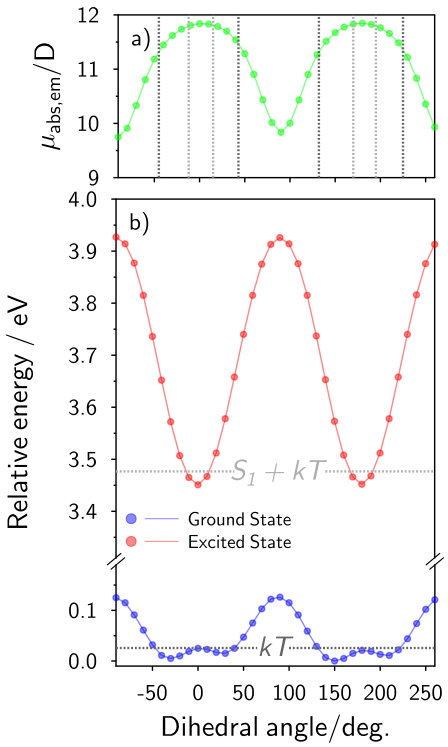

Figure S28: Effect of the dihedral angle between the central thiophene and an adjacent phenyl subunit on a) the $S_1 \leftrightarrow S_0$ transition dipole moment, $\mu_{abs,em}$, and b) the energy of the ground state and S_1 state of **1** (CAM-B3LYP/cc-VDZ with GD3 empirical dispersion, gas phase). Dark grey line shows kT relative to the ground state, light grey line shows $S_1 + kT$. Dark grey lines in a) show range of absorption transition dipole moment, light grey showing range of emission transition dipole moment.

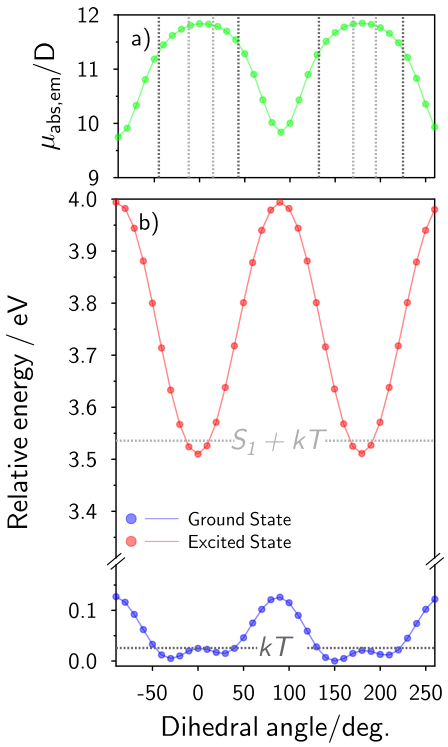

Figure S29: Effect of the dihedral angle between the central thiophene and an adjacent phenyl subunit on a) the $S_1 \leftrightarrow S_0$ transition dipole moment, $\mu_{abs,em}$, and b) the energy of the ground state and S_1 state of **2** (CAM-B3LYP/cc-VDZ with GD3 empirical dispersion, gas phase). Dark grey line shows kT relative to the ground state, light grey line shows $S_1 + kT$. Dark grey lines in a) show range of absorption transition dipole moment, light grey showing range of emission transition dipole moment.

4.2 Simulation of Symmetry Breaking

To simulate the effect of the localization of the excitation on a single branch of **1** on the emission transition dipole, μ_{em}, TD-DFT calculations of the $S_1 \leftarrow S_0$ transition dipole moment, μ_{abs}, were performed with **1** and with the single branch analogue, **1'**. The results are listed in table S4. Upon going from **1** to **1'**, μ_{abs} is predicted to decrease by 40 %. By analogy, localization of the excitation on a single branch of **1** upon symmetry breaking should lead to a similar decrease of μ_{em}. The frontier molecular orbitals of **1** and **1'** are depicted in Figures S30, S31, S32 and S33.

Table S4: Calculated parameters from TD-DFT for 1 and 1-branch analogue 1'.

Compound	S_1 energy/eV	Oscillator Strength	μ_{abs}/D	HOMO-LUMO transition %
1	3.57	1.85	11.7	82
1'	4.00	0.78	7.2	84

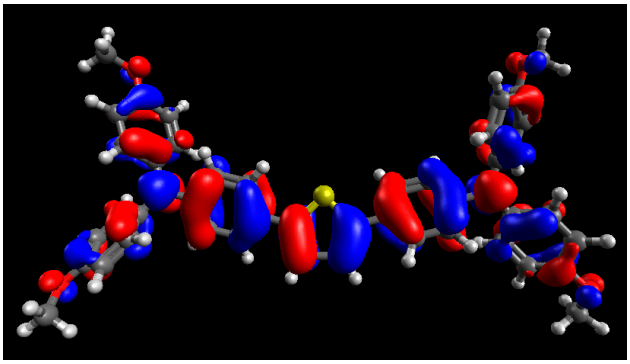

Figure S30: HOMO of **1** computed at the DFT level.

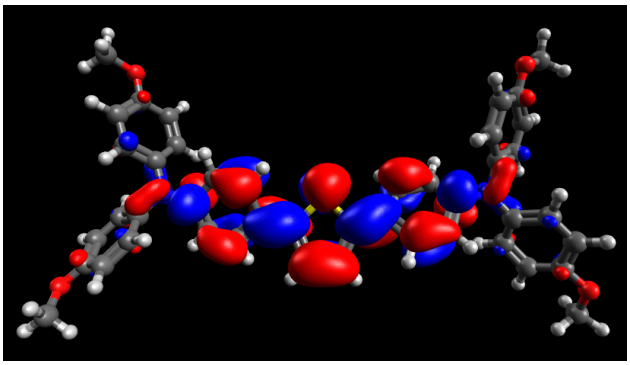

Figure S31: LUMO of **1** computed at the DFT level.

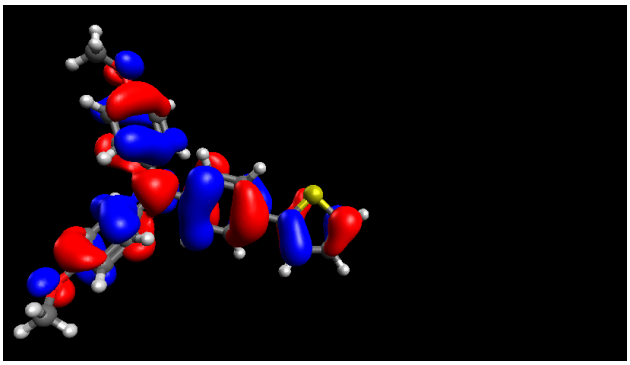

Figure S32: HOMO of **1'** computed at the DFT level.

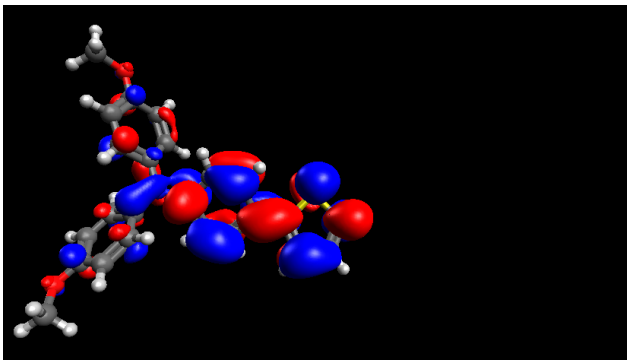

Figure S33: LUMO of **1'** computed at the DFT level.

References

(1) Gardecki, J. A.; Maroncelli, M. Set of Secondary Emission Standards for Calibration of the Spectral Responsivity in Emission Spectroscopy. *Appl. Spectrosc.* **1998**, *52*, 1179–1189.

(2) Magde, D.; Wong, R.; Seybold, P. G. Fluorescence Quantum Yields and Their Relation to Lifetimes of Rhodamine 6G and Fluorescein in Nine Solvents: Improved Absolute Standards for Quantum Yields. *Photochem. Photobiol.* **2002**, *75*, 327–334.

(3) Breffke, J.; Williams, B. W.; Maroncelli, M. The Photophysics of Three Naphthylmethylene Malononitriles. *J. Phys. Chem. B* **2015**, *119*, 9254–9267.

(4) Kubista, M.; Sjöback, R.; Eriksson, S.; Albinsson, B. Experimental Correction for the Inner-Filter Effect in Fluorescence Spectra. *Analyst* **1994**, *119*, 417–419.

(5) Makarov, N. S.; Drobizhev, M.; Rebane, A. Two-Photon Absorption Standards in the 550–1600 nm Excitation Wavelength Range. *Opt. Express, OE* **2008**, *16*, 4029–4047.

(6) Ceymann, H.; Rosspeintner, A.; Schreck, M. H.; Mützel, C.; Stoy, A.; Vauthey, E.; Lambert, C. Cooperative Enhancement versus Additivity of Two-Photon-Absorption Cross Sections in Linear and Branched Squaraine Superchromophores. *Phys. Chem. Chem. Phys.* **2016**, *18*, 16404–16413.

(7) de Reguardati, S.; Pahapill, J.; Mikhailov, A.; Stepanenko, Y.; Rebane, A. High-Accuracy Reference Standards for Two-Photon Absorption in the 680–1050 Nm Wavelength Range. *Opt. Express, OE* **2016**, *24*, 9053–9066.

(8) Muller, P.-A.; Högemann, C.; Allonas, X.; Jacques, P.; Vauthey, E. Deuterium Isotope Effect on the Charge Recombination Dynamics of Contact Ion Pairs Formed by Electron-Transfer Quenching in Acetonitrile. *Chem. Phys. Lett.* **2000**, *326*, 321–327.

(9) Zhang, X.-X.; Würth, C.; Zhao, L.; Resch-Genger, U.; Ernsting, N. P.; Sajadi, M. Femtosecond Broadband Fluorescence Upconversion Spectroscopy: Improved Setup and Photometric Correction. *Rev. Sci. Instrum.* **2011**, *82*, 063108.

(10) Gerecke, M.; Bierhance, G.; Gutmann, M.; Ernsting, N. P.; Rosspeintner, A. Femtosecond Broadband Fluorescence Upconversion Spectroscopy: Spectral Coverage versus Efficiency. *Rev. Sci. Instrum.* **2016**, *87*, 053115.

(11) Yanai, T.; Tew, D. P.; Handy, N. C. A New Hybrid Exchange–correlation Functional Using the Coulomb-Attenuating Method (CAM-B3LYP). *Chem. Phys. Lett.* **2004**, *393*, 51–57.

(12) Frisch, M.; Trucks, G.; Schlegel, H.; Scuseria, G.; Robb, M.; Cheeseman, J.; Scalmani, G.; Barone, V.; Mennucci, B.; Petersson, G. et al. Gaussian 09, Revision D. *Gaussian 09 Revis. Gaussian Inc Wallingford CT 2016* **2009**,

(13) Grimme, S.; Antony, J.; Ehrlich, S.; Krieg, H. A Consistent and Accurate *Ab Initio* Parametrization of Density Functional Dispersion Correction (DFT-D) for the 94 Elements H-Pu. *J. Chem. Phys.* **2010**, *132*, 154104.

(14) Bauernschmitt, R.; Ahlrichs, R. Treatment of Electronic Excitations within the Adiabatic Approximation of Time Dependent Density Functional Theory. *Chem. Phys. Lett.* **1996**, *256*, 454–464.

(15) Stratmann, R. E.; Scuseria, G. E.; Frisch, M. J. An Efficient Implementation of Time-Dependent Density-Functional Theory for the Calculation of Excitation Energies of Large Molecules. *J. Chem. Phys.* **1998**, *109*, 8218–8224.

(16) Scalmani, G.; Frisch, M. J.; Mennucci, B.; Tomasi, J.; Cammi, R.; Barone, V. Geometries and Properties of Excited States in the Gas Phase and in Solution: Theory and Application of a Time-Dependent Density Functional Theory Polarizable Continuum Model. *J. Chem. Phys.* **2006**, *124*, 094107.

(17) Navarro, O.; Nolan, S. P. Large-Scale One-Pot Synthesis of N-Heterocyclic Carbene-Pd(Allyl)Cl Complexes. *Synthesis* **2006**, *2006*, 366–367.

(18) Brisset, H.; Thobie-Gautier, C.; Gorgues, A.; Jubault, M.; Roncali, J. Novel Narrow Bandgap Polymers from Sp3 Carbon-Bridged Bithienyls: Poly(4,4-Ethylenedioxy-4H-Cyclopenta[2,1-b;3,4-B′]Dithiophene). *J. Chem. Soc., Chem. Commun.* **1994**, *0*, 1305–1306.

(19) Lumpi, D.; Holzer, B.; Bintinger, J.; Horkel, E.; Waid, S.; Wanzenböck, H. D.; Marchetti-Deschmann, M.; Hametner, C.; Bertagnolli, E.; Kymissis, I. et al. Substituted Triphenylamines as Building Blocks for Star Shaped Organic Electronic Materials. *New J. Chem.* **2015**, *39*, 1840–1851.

(20) Marion, N.; Navarro, O.; Mei, J.; Stevens, E. D.; Scott, N. M.; Nolan, S. P. Modified (NHC)Pd(Allyl)Cl (NHC = N-Heterocyclic Carbene) Complexes for Room-Temperature Suzuki-Miyaura and Buchwald-Hartwig Reactions. *J. Am. Chem. Soc.* **2006**, *128*, 4101–4111.

(21) Holzer, B.; Lunzer, M.; Licari, G.; Tromayer, M.; Naumov, S.; Lumpi, D.; Horkel, E.; Hametner, C.; Rosspeintner, A.; Liska, R. et al. Initiators for Two-Photon Induced Polymerization Based on a Novel Cap-Linker-Cap System. *Manuscript in Preparation*

(22) Birks, J. B. *Photophysics of Aromatic Molecules*; Wiley monographs in chemical physics; Wiley-Interscience: London, New York, 1970.

(23) Toptygin, D. Effects of the Solvent Refractive Index and Its Dispersion on the Radiative Decay Rate and Extinction Coefficient of a Fluorescent Solute. *J Fluoresc* **2003**, *13*, 201–219.

(24) Arzhantsev, S.; Zachariasse, K. A.; Maroncelli, M. Photophysics of Trans-4-(Dimethylamino)-4‘-Cyanostilbene and Its Use as a Solvation Probe. *J. Phys. Chem. A* **2006**, *110*, 3454–3470.

(25) Marcus, Y. *The Properties of Solvents*; Wiley series in solution chemistry v. 4; Wiley: Chichester ; New York, 1998.

(26) Angulo, G.; Grampp, G.; Rosspeintner, A. Recalling the Appropriate Representation of Electronic Spectra. *Spectrochim. Acta A* **2006**, *65*, 727–731.